ACS APPLIED MATERIALS & INTERFACES

Research Article

www.acsami.org

Construction and Evaluation of Fe_3O_4-Based PLGA Nanoparticles Carrying rtPA Used in the Detection of Thrombosis and in Targeted Thrombolysis

Jun Zhou,[†] Dajing Guo,*[,†] Yu Zhang,[†] Wei Wu,[†] Haitao Ran,[‡] and Zhigang Wang[‡]

[†]Department of Radiology, and [‡]Institute of Ultrasound Imaging, Department of Ultrasound, Second Affiliated Hospital of Chongqing Medical University, No. 74 Linjiang Rd, Yuzhong District, 400010 Chongqing, China

Supporting Information

ABSTRACT: Thrombotic disease is extremely harmful to human health, but early detection and treatment can help improve prognoses and reduce mortality. To date, few studies have used MR molecular imaging in the early detection of thrombi and in the dynamic monitoring of the thrombolytic efficiency. In this article, we construct Fe_3O_4-based poly(lactic-co-glycolic acid) (PLGA) nanoparticles to use in the detection of thrombi and in targeted thrombolysis using MRI monitoring. Cyclic arginine-glycine-aspartic peptide (cRGD) was grafted onto the chitosan (CS) surface to synthesize a CS-cRGD film using carbodiimide-mediated amide bond formation. A double emulsion solvent evaporation method (water in oil in water [W/O/W]) was used to construct Fe_3O_4-based PLGA nanoparticles carrying recombinant tissue plasminogen activator (rtPA) (Fe_3O_4−PLGA-rtPA/CS-cRGD). Fe_3O_4−PLGA, Fe_3O_4−PLGA-rtPA, and Fe_3O_4−PLGA-rtPA/CS nanoparticles were constructed using the same W/O/W method. The results showed that the Fe_3O_4-based nanoparticles were constructed successfully and have a regular shape, a relatively uniform size, a high carrier rate of Fe_3O_4 and encapsulation efficiency of rtPA, and a relatively high activity of released rtPA. Transmission electron microscope (TEM) images revealed that the iron oxide particles were relatively uniformly distributed in the nano-spherical shell. The Fe_3O_4-based nanoparticles could be imaged using a clinical MRI scanner, and there were no significant differences in the transverse relaxation rate (R_2*) or in the signal-to-noise ratio (SNR) values between the Fe_3O_4-based nanoparticles and an Fe_3O_4 solution with the same concentration of Fe_3O_4. In vitro and in vivo experiments confirmed that the Fe_3O_4−PLGA-rtPA/CS-cRGD nanoparticles specifically accumulated on the edge of the thrombus and that they had a significant effect on the thrombolysis compared with the Fe_3O_4−PLGA, Fe_3O_4−PLGA-rtPA, and Fe_3O_4−PLGA-rtPA/CS nanoparticles and with free rtPA solution. These results suggest the potential of the Fe_3O_4−PLGA-rtPA/CS-cRGD nanoparticles as a dual-function tool in the early detection of a thrombus and in the dynamic monitoring of the thrombolytic efficiency using MRI.

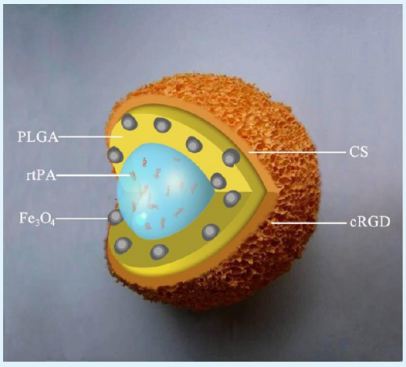

KEYWORDS: *iron oxide, poly(lactic-co-glycolic acid), thrombolysis, nanoparticle, cyclic arginine-glycine-aspartic peptide, recombinant tissue plasminogen activator*

1. INTRODUCTION

Thrombotic disease is a leading cause of death and disability in developed countries, but the early diagnosis and treatment of thrombosis can effectively reduce the morbidity and mortality rates.[1] Intravenous thrombolytic therapy is the main choice in the treatment of thrombosis. The various thrombolytic drugs used clinically have complications such as a short half-life in plasma, a low targeting ability, and the tendency to cause hemorrhage; thus, local thrombolytic therapy is attractive. In this method, thrombolytic drugs are loaded into a carrier system and systemically transported to the thrombus site using a variety of targeting methods, at which point they induce targeted thrombolysis, thus reducing the amount of thrombolytic drugs needed and the complications of hemorrhage and reembolism that are caused by thrombolytic drugs.

Previous studies have reported a variety of particles that have been used in targeted thrombolysis including liposome-encapsulated tissue plasminogen activator (tPA),[2] SonoVue microbubbles carrying urokinase that were used in the treatment of thrombi with the aid of ultrasound irradiation,[3] magnetic nanoparticles carrying thrombolytic drugs that were used in magnetic targeting therapy,[4−7] and poly (lactic-co-glycolic acid) (PLGA) used as a carrier in targeted thrombolysis.[8,9] However, few reports have employed a new type of molecular probe in the treatment as well as in the diagnosis of the thrombi. Compared with the methods that use ultrasound and nuclear medicine, high-resolution MR molecular imaging without radiation and with the ability to obtain 3D information about the anatomic structure and physiology has attracted attention in recent years, which has led to the

Received: December 27, 2013
Accepted: March 21, 2014
Published: March 21, 2014

proliferation of MR molecular imaging. The targeted detection of thrombi and the dynamic monitoring of the thrombolytic efficiency using MRI have great future potential. To the best of our knowledge, no one has reported the construction of PLGA nanoparticles loaded with an MR contrast agent and the in vivo targeted detection of a thrombus as well as the dynamic monitoring of the thrombolytic efficiency.

PLGA has attracted attention as a carrier material and has been widely used due to its biocompatibility and biodegradability; the U.S. Food and Drug Administration (FDA) and the European Medicine Agency (EMA) have approved the use of PLGA in the parenteral administration of a drug carrier system.[10−12] PLGA is usually used in the construction of intravenous drug delivery formulations and of biomimetic materials and has extensive application prospects in drug delivery systems, the diagnosis and treatment of disease, medical imaging, and tissue engineering.[13−16]

In recent years, studies have successfully encapsulated the MR contrast agents gadolinium diethylenetriaminepentaacetic acid (Gd-DTPA) and superparamagnetic iron oxide (SPIO) into macromolecular polymer particles to construct a new type of MR contrast agent.[17−23] These MR contrast agents were confirmed to have a low biological toxicity by studying their physical and chemical characteristics and their distribution and degradation in vivo in animals. They could be imaged on a clinical MR scanner, and their imaging capabilities were similar to those when Gd-DTPA or SPIO was used separately. The MR contrast agent SPIO, a nanoparticle formed by γ-Fe_2O_3 and Fe_3O_4 that have been coated with various substances, can produce a strong T_2 negative contrast effect. Compared with Gd-DTPA, SPIO has the advantages of a long half-life, a high relaxation rate and low drug side effects. It can be converted to Fe^{2+} or Fe^{3+} in the plasma iron pool in the body, thereby participating in the processes of human red blood cells as well as other metabolic processes, and it is now widely used in MR molecular imaging.[24]

The specific binding of activated platelets and fibrinogen is part of the final pathway of thrombosis. Arg-Gly-Asp (RGD) peptide is a receptor antagonist of platelet membrane glycoprotein GP IIb/IIIa, and it has a tendency to bind activated platelets at the thrombus site, to adhere to the surface of the thrombus, and, through competition with fibrinogen, to restrain the platelets from accumulating.[25] Previous studies reported that RGD peptide was bound to the surface of liposome microbubbles, where it targeted activated platelets.[25,26] Hua et al. reported that RGDS peptides surface-conjugated to tPA-loaded liposome microbubbles could enhance in vitro thrombolysis.[2] Mu et al. successfully connected urokinase and RGDS to the surface of SonoVue microbubbles to use in in vitro targeted thrombolysis.[3] GRGD peptide-grafted chitosan (CS) has also been used as a surface modifier in PLGA particles loaded with thrombolytic drugs to investigate the possible effects on targeted thrombolysis.[8,9] Tang et al. proved that cyclic RGD (cRGD) possessed a higher affinity for the platelet membrane glycoprotein GP IIb/IIIa compared with linear RGD.[27]

As a representative of the selective thrombolytic drugs, recombinant tissue plasminogen activator (rtPA) can combine with fibrin close to fibrin-plasminogen combining sites, transforming the plasminogen into plasmin at the thrombus site without activating the free plasminogen in the blood. Compared with urokinase and streptokinase, the thrombolytic drugs widely used in clinical treatment of thrombosis, rtPA, with its advantages of high selectivity to thrombosis, good thrombolytic effect, and non-immunogenicity, has been widely used in the treatment of acute myocardial infarction and cerebral thrombus lesions. As reported in the literature, rtPA has been covalently bound to the surface of magnetic nanoparticles[5−7] or wrapped in PLGA nanoparticles[8,9] to target thrombolysis, actions that could enhance its thrombolytic effect.

In this study, the ligand cRGD was grafted onto CS surfaces to synthesize a CS-cRGD film using carbodiimide-mediated amide bond formation. PLGA was employed as the core of the drug carrier, and a double emulsion solvent evaporation method (water in oil in water [W/O/W]) was used to construct the PLGA nanoparticles. Fe_3O_4 with a surface modification of oleic acid was embedded in the layer of PLGA as an organic phase, and the thrombolytic drug rtPA was wrapped inside the nanoparticles as an inner aqueous phase. The CS-cRGD film was added to the outer aqueous phase during the preparation procedure. By changing the component part of the organic phase and the inner and outer aqueous phases, Fe_3O_4−PLGA, Fe_3O_4−PLGA-rtPA, Fe_3O_4−PLGA-rtPA/CS, and Fe_3O_4−PLGA-rtPA/CS-cRGD nanoparticles were constructed using the same method. Our purpose was to construct thrombus-targeting nanoparticles with a dual function of the early detection and the treatment of a thrombus. In addition, under the monitoring of MRI, we aimed to investigate the characteristics of the nanoparticles related to their ability to target a thrombus and induce thrombolysis with the expectation of achieving a precise positioning of the thrombi and both qualitative detection and dynamic monitoring of the thrombolytic efficiency during in vitro and in vivo experiments.

2. MATERIALS AND METHODS

2.1. Materials. PLGA (containing 75% lactide and 25% glycolide) with a MW of 20 000 was purchased from Jinan Daigang Biological Material Co., Ltd (Shangdong, China). Iron oxide nanoparticles that had been surface modified with oleic acid (Fe_3O_4) were purchased from Ocean Nano Technology Co., Ltd (Springdale, AR, USA). rtPA was purchased from Boehringer Ingelheim (Ingelheim, Germany). cRGD peptide was synthesized by GL Biochem (Shanghai, China). CS (M_v 140 000−220 000) with 93% deacetylation and a characteristic viscosity of 5−200 mPa s (1 % solution in 1 % HAc), polyvinyl alcohol (PVA) with an average MW of 30 000−70 000, 1-ethyl-3-(3-dimethylaminopropyl) carbodiimide hydrochloride (EDC), and N-hydroxysuccinimide (NHS) were obtained from Sigma-Aldrich Corporation (St Louis, MO, USA). The protease substrate H-D-Isoleucyl-L-prolyl-L-arginine-*p*-nitroaniline (S-2288) was provided by Chromogenix (Milan, Italy). All other reagents used were at least of analytical grade.

2.2. Preparation of the CS and CS-cRGD Films. To prepare the CS film, 100 mg of CS was dissolved in 10 mL of 1% acetic acid solution, stirred until it was fully dissolved, degassed using ultrasound, and poured into a polytetrafluoroethylene mold, which was placed in an oven at 40 °C to dry after the cast became flat; then the CS film was removed and soaked in a 5 % NaOH solution for half an hour, flushed repeatedly using distilled water until its pH 7, and dried naturally before being stored. The CS-cRGD film was synthesized following a method described elsewhere.[28] In this method, an appropriate amount of EDC and NHS with a molar ratio of 1.5:1 was added to a PBS buffer solution. The pH was adjusted to 7 using an NaOH solution, and 0.05 mmol of cRGD peptide and CS film were added and allowed to react for 24 h at 4 °C to form the CS-cRGD film. Finally, the CS-cRGD film was rinsed with distilled water to remove the unreacted materials and air-dried at room temperature.

2.3. Preparation of the Fe_3O_4-Based PLGA Nanoparticles. The W/O/W method was used to prepare the Fe_3O_4-based PLGA

nanoparticles but was modified based on reports in the literature.[22,23,28] First, 100 mg of PLGA and 100 μL of Fe_3O_4 were fully dissolved in 2 mL of dichloromethane (organic phase, O); then, 0.4 mL of double-distilled water (inner aqueous phase, W_1) was added. Acoustic vibration for 60 s using an ultrasonic oscillation instrument (VCX130, Sonics & Materials, Inc., Newtown, CT, USA) produced a brown emulsion that was poured into 10 mL of 3 % PVA solution (outer aqueous phase, W_2) and homogenized at 15 000 rpm for 5 min with a high-speed homogenization dispersion machine (C10, Shanghai HENC mechanical equipment company, Shanghai, China) to produce a double emulsion solution. Then, 20 mL of 2 % isopropanol solution was added and stirred continuously at room temperature for 2 h until the surface solidification of the nanoparticles and the volatilization of the dichloromethane occurred. The Fe_3O_4–PLGA nanoparticles were collected, frozen, and dried for storage after centrifugation using a high-speed refrigerated centrifuge (Centrifuge 5804R, Eppendorf, Germany), rinsing with double-distilled water, and removing the supernatant. All of the supernatant was collected.

To fabricate the Fe_3O_4–PLGA-rtPA nanoparticles, the same procedures were used that were followed when preparing the Fe_3O_4-PLGA nanoparticles except that 0.2 mL of 1 mg/mL rtPA solution rather than 0.4 mL of double distilled water was added as the inner aqueous phase, W_1, to the aforementioned organic phase, O, following the preparation of the Fe_3O_4–PLGA nanoparticles. During the preparation of the rtPA-containing nanoparticles, samples were placed in an ice bath to avoid the inactivation of the rtPA. To fabricate the Fe_3O_4–PLGA-rtPA nanoparticles that were coated with a film of CS or CS-cRGD, which were dissolved in 0.5 % acetic acid solutions, the same procedures were followed as in preparing the Fe_3O_4–PLGA-rtPA nanoparticles except that 5 mL of CS or CS-cRGD solution and 5 mL of 3% PVA solution were added as the outer aqueous phase, W_2, rather than the 10 mL of PVA solution (Figure 1). Furthermore, the pH

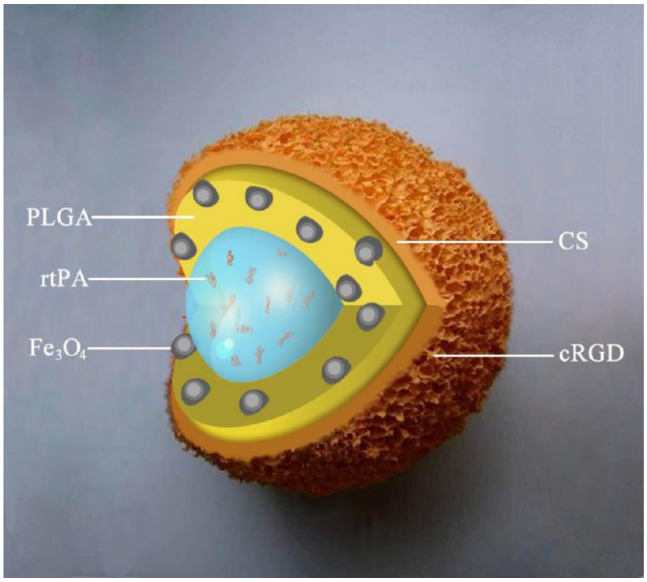

Figure 1. Schematic representation of an Fe_3O_4–PLGA-rtPA/CS-cRGD nanoparticle. The structure of the nanoparticle is briefly described as follows: the core of the first emulsion was an rtPA solution encapsulated in a shell of PLGA and Fe_3O_4, and a CS-cRGD film was coated on the surface of the PLGA-Fe_3O_4 layer using the W/O/W method.

value of the emulsion was adjusted to 6–7 during the evaporation of the solvent to enhance the formation of the CS or CS-cRGD coating on the PLGA nanoparticles.

2.4. Physical and Chemical Characteristics. *2.41. Morphology, Structure, Size, and Zeta Potential of the Different Nanoparticles.* After the appropriate nanoparticles were dissolved in double-distilled water, their morphology, surfaces, and dispersion were observed using an optical microscope (Olympus CKX41, Olympus Co. Ltd., Tokyo, Japan), and the internal structures were observed using a transmission electron microscope (TEM) (Hitachi 7500, Hitachi Ltd., Tokyo, Japan). The application of the CS-cRGD film onto the PLGA nanoparticles was confirmed using laser scanning confocal microscopy (Leica TCS-SP2, Leica Microsystems, Wetzlar, Germany). The cRGD was labeled with FITC. The sizes, polydispersity indexes (PDIs), and zeta potentials of the different nanoparticles were determined at 25 °C using a laser particle size analyzer (Zetasizer Nano ZS90, Malvern Instruments Ltd, Worcs, UK).

2.42. Carrier Rate of the Fe_3O_4 and cRGD in the Fe_3O_4-Based PLGA Nanoparticles. The Fe_3O_4 concentration was analyzed using an atomic absorption spectrometer (Hitachi model Z-5000, Hitachi Ltd., Tokyo, Japan). First, 10 mg of a lyophilized powder of magnetic PLGA nanoparticles was dissolved in 1 mL of dimethylsulfoxide to dissolve the PLGA nanoparticles. Then, 1 mL of 36 % HCl was added to decompose the Fe_3O_4, the free Fe ion was obtained, and the solution was diluted to a volume of 10 mL using 1 % HCl. The carrier rate of the Fe_3O_4 was found using the following formula: the carrier rate of Fe_3O_4 (%) = (the mass of Fe_3O_4 in the sample)/(the total mass of added Fe_3O_4) × 100 %.

The carrier rate of the cRGD was measured using flow cytometry (FACSVantage SE, Becton Dickinson, San Jose, CA, USA). We randomly counted 10,000 nanoparticles and measured the carrier rate of the cRGD.

2.43. Encapsulation Efficiency and Activity of the rtPA in the Fe_3O_4-Based PLGA Nanoparticles. The concentration of the rtPA in the supernatant was determined using a colorimetric method at 595 nm with the Protein Assay Kit from Bio-Rad. The encapsulation efficiency of the rtPA (%) = (the amount of added rtPA − the amount of rtPA in the supernatant)/(the total amount of added rtPA) × 100%. S-2288, a specific chromogenic substrate for rtPA, was used to analyze the activity of the rtPA. Briefly, 5 mg of nanoparticles was dispersed in 1 mL of PBS maintained at 37 °C in a water bath; the nanoparticles were separated from the solution using centrifugation at 7500 rpm every 5 min, and then 0.5 mL of supernatant was extracted to determine the activity of the released rtPA using S-2288; finally, 0.5 mL of PBS was added, and the nanoparticles were placed back in the 37 °C water bath. The measurement of the activity of the released rtPA was performed three times.

2.5. In Vitro Experiment Used to Target a Thrombus and Monitor Thrombolysis. Peripheral vein blood was collected from a healthy volunteer according to an IRB-approved protocol after obtaining informed consent. Blood clots were formed in coagulation-promoting vacuum tubes in a 37 °C water bath for 2 h. The Fe_3O_4–PLGA, Fe_3O_4–PLGA-rtPA, Fe_3O_4–PLGA-rtPA/CS, and Fe_3O_4–PLGA-rtPA/CS-cRGD nanoparticles were dissolved in a PBS buffer solution; then a blood clot with an approximate diameter of 9 mm was added to each solution. After incubation at 37 °C in a water bath for 15 min, the blood clots were rinsed repeatedly with the PBS buffer solution at a flow rate of 20 cm/s for 1 min, and then a pathologically frozen section was created to observe the targeting ability of the nanoparticles at the thrombus using an optical microscope.

In the in vitro thrombolysis experiment, the blood clots were cut into pieces of 100 mg in weight. Each blood clot was weighed on an electronic balance (XS104, Mettler Toledo Co., Switzerland) before the thrombolysis and at 15 min, 30 min, and 60 min after the thrombolysis began. All the clots placed into glass tubes were treated with one of five materials: Fe_3O_4–PLGA nanoparticles, free rtPA solution, and Fe_3O_4–PLGA-rtPA, Fe_3O_4–PLGA-rtPA/CS, and Fe_3O_4–PLGA-rtPA/CS-cRGD nanoparticles. The nanoparticles that encapsulated rtPA were dissolved in a PBS buffer solution with the same rtPA content as the free rtPA solution. The nanoparticles and the free rtPA solution were injected through the glass tube upstream of the clot and then washed through the region of the clot within the tube via a peristaltic pump at a flow rate of 1 mL/min. The clots were then washed using a sustained flow of saline solution propelled by the peristaltic pump (Figure 2). The thrombolysis rate was calculated as the percentage ratio of the difference in weights to the initial weight.

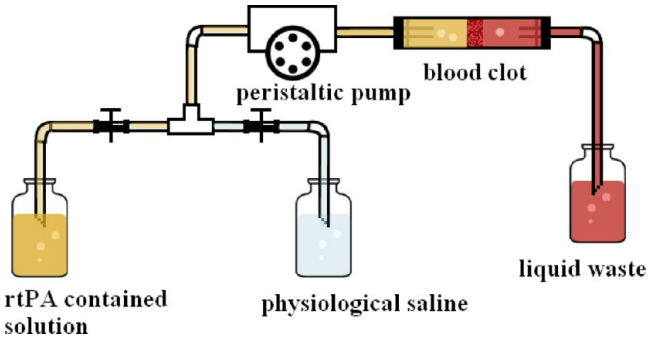

Figure 2. Illustration of the flow model used in the in vitro thrombolysis.

The thrombolysis rate (%) = (the weight of clots before thrombolysis − the weight of clots after thrombolysis)/(the weight of clots before thrombolysis) × 100 %.

2.6. MRI Characterization of the Fe_3O_4-Based PLGA Nanoparticles. To assess the contrast enhancement of the Fe_3O_4-based PLGA nanoparticles, six materials were used: 0.9 % agarose solution, Fe_3O_4−PLGA, Fe_3O_4−PLGA-rtPA, Fe_3O_4−PLGA-rtPA/CS, Fe_3O_4−PLGA-rtPA/CS-cRGD, and Fe_3O_4 solution. As the PLGA nanoparticles were prone to sink in water, each material that contained nanoparticles was embedded in a 0.9% agarose solution and placed in an Eppendorf tube, and each had the same concentration of Fe_3O_4 (0.01 μmol/L). The total volume of each solution was 4 mL. To avoid susceptibility artifacts from the surrounding air in the images, all the suspensions were placed in a plastic container filled with water. An MR scan was performed using a 1.5 T MR scanner (HDXT2012, GE Medical Systems, Fairfield, CT, USA), a skull-dedicated single-channel quadrature coil, and a T_2*-weighted pulse sequence with the following parameters: gradient echo (GRE) sequence, repetition time (TR) = 520 ms, echo time (TE) = 10.7 ms, flip angle (FA) = 45°, and slice thickness = 3 mm. The MR imaging experiments were performed three times with each contrast agent. The mean signal intensities (SIs) of the nanoparticles were measured in the central section of the imaging volume by one investigator using operator-defined regions of

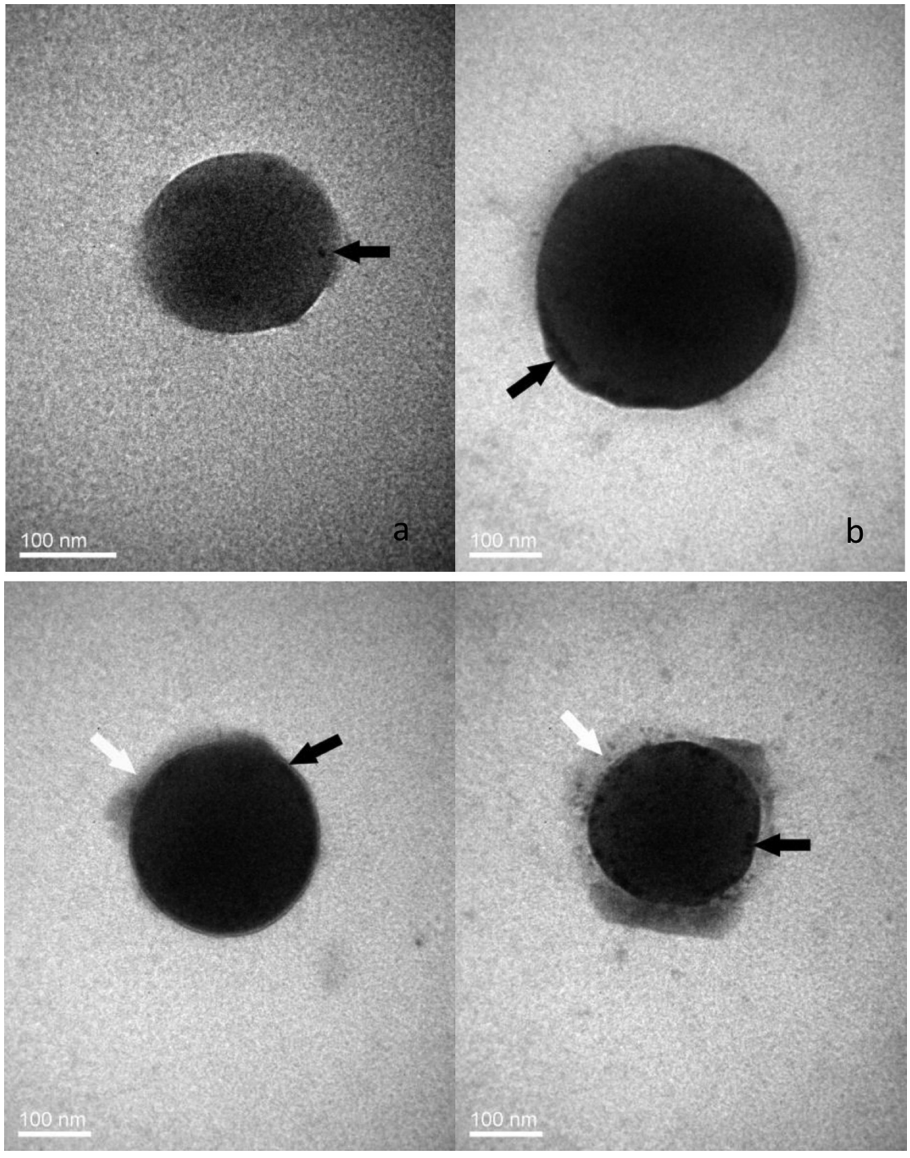

Figure 3. TEM images of the (a) Fe_3O_4−PLGA, (b) Fe_3O_4−PLGA-rtPA, (c) Fe_3O_4−PLGA-rtPA/CS, and (d) Fe_3O_4−PLGA-rtPA/CS-cRGD nanoparticles. The iron oxide particles (black arrows) were relatively uniformly distributed in the nano-spherical shell, and the CS film (white arrows) was observed around the nanoparticles that had been coated with a CS or CS-cRGD film.

interest (ROIs) with a minimum of 100 pixels. The SI data were divided by the background noise to yield the signal-to-noise ratio (SNR): SNR = SI/noise. The differences in the SNR values were analyzed.

Because of the superparamagnetic properties of Fe_3O_4, only the transverse relaxation rate (R_2*) was calculated. Pure Fe_3O_4 was diluted with chloroform. Suspended nanoparticles containing Fe_3O_4 were dissolved in a 0.9 % agarose solution and compared with solutions of unencapsulated Fe_3O_4 with the same concentrations. Reference samples of each contrast agent at increasing dilutions of the iron oxides (0.01−0.05 μmol/L Fe_3O_4) were imaged. MRI was performed using a 1.5 T MR scanner, a head coil, and a T_2*-weighted pulse sequence with the following parameters: TR = 35 ms, 16 increasing TE from 1.5 to 18.8 ms, matrix 320 × 192, number of excitations (NEX) = 1, and slice thickness =1.5 mm. The data were transferred to an ADW4.2 image workstation, and the Research R_2* software package was used to measure the R_2* values. This experiment was performed three times. The R_2* value of each group was measured with an ROI of 100 pixels, and the average was taken as the final value.

2.7. MRI of the in Vitro Targeting of the Thrombus. MRI of the in vitro targeting of the thrombus was performed after the blood clots were incubated with different nanoparticles. The T_2*-weighted fast field echo (FFE) sequence was acquired using a 3.0 T MRI scanner (Achieva 3.0 T TX, Philips Healthcare, Best, the Netherlands) and a rat experiment coil (CG-MUC 18-H300-AP, Shanghai Chenguang Medical Technologies Co., Ltd., Shanghai, China). The imaging parameters were TR = 119 ms, TE = 9 ms, FA = 45°, field of view (FOV) = 60 mm, matrix 512 × 256, and slice thickness = 1 mm. To characterize the deposition of the nanoparticles at the target, we suspended each of 3 blood clots with an approximate size of 9 mm in a PBS solution in a plastic tube. The clots were incubated with the Fe_3O_4−PLGA-rtPA, Fe_3O_4−PLGA-rtPA/CS, or Fe_3O_4−PLGA-rtPA/CS-cRGD nanoparticles. Each blood clot was removed after 15 min of incubation, placed in a plastic tube, and rinsed with a PBS buffer solution at a flow rate of 20 cm/s for 1 min. All the blood clots were placed in 25-mL beakers and embedded in a 0.9 % agarose solution to avoid the movement of artifacts during the MR scan.

2.8. MRI of in Vivo Targeted Thrombolysis. The animal studies were approved by the Animal Center of Chongqing Medical University. In vivo thrombi were induced using a ferric chloride ($FeCl_3$) injury to the abdominal aorta. SD rats that weighed between 180 and 200 g each were anesthetized using chloral hydrate. After the abdominal aorta was exposed, a filter paper saturated with a 10 % $FeCl_3$ solution was used to cover the abdominal aorta region for 3−5 min; during this process, parafilm was placed between the filter film and the abdominal wall to prevent any leakage of the $FeCl_3$ to the surrounding tissues. When the thrombus had formed in the injured artery, the filter film and parafilm were removed and the abdominal cavity was sutured after washing it with saline. The MR scans of the SD rats were performed using a 3.0 T MR scanner with a rat experiment coil before and after the $FeCl_3$ injury to the abdominal aorta and then 10 min, 20 min, 40 min, and 60 min after the intravenous injection of 5 mg of a lyophilized powder of the Fe_3O_4−PLGA-rtPA or Fe_3O_4−PLGA-rtPA/CS-cRGD nanoparticles dissolved in 1 mL of PBS buffer solution. The T_2-weighted sequence was performed using the following parameters: TR = 666 ms, TE = 62 ms, FA = 90°, FOV = 50 mm, and slice thickness = 1 mm. The Vs3DI sequence was performed using the following parameters: TR = 20 ms, TE = 3 ms, FA = 12°, and FOV = 60 mm.

2.9. Statistical Analysis. The data were analyzed using the Statistical Program for Social Sciences (SPSS for Windows, version 17.00, Chicago, IL, USA). The continuous variables were presented as the mean ± the standard deviation, and the categorical variables were reported numerically and as percentages. One-way ANOVA and independent sample *t*-tests were used to compare the differences in the SNR, the R_2* values, the cumulative activity of the released rtPA, and the thrombolysis rates among the different nanoparticles. The statistical significance was defined at $P < 0.05$.

3. RESULTS

3.1. Characteristics of the Fe_3O_4-Based PLGA Nanoparticles. The nanoparticles described above were successfully constructed using the W/O/W method. Optical microscopy showed relatively homogeneous particle sizes among the nanoparticles with spherical, smooth surfaces and good dispersions. TEM revealed that the iron oxide particles were relatively uniformly distributed in the nanospherical shell, and the CS film was observed around the nanoparticles (Figure 3). Confocal laser microscopy showed annular green fluorescent materials around the Fe_3O_4−PLGA-rtPA/CS-cRGD nanoparticles; however, almost no fluorescent material was detected within the inner aqueous phase, which demonstrated that the CS-cRGD that was labeled with FITC was successfully coated onto the surface of the PLGA nanoparticles (Figure 4). The

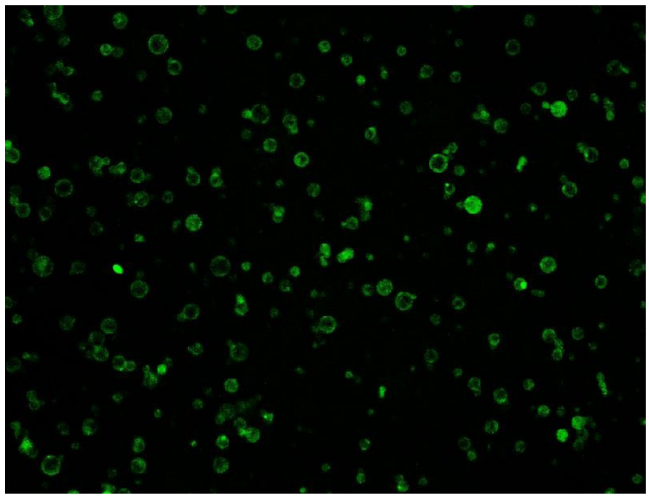

Figure 4. Laser scanning confocal microscopy image of the Fe_3O_4−PLGA-rtPA/CS-cRGD nanoparticles. Annular green fluorescence was observed around the nanoparticles, but almost no fluorescence was found in the inner aqueous phase.

average particle diameters, PDIs, zeta potentials, carrier rates of Fe_3O_4, and rtPA-encapsulation efficiencies of the nanoparticles are shown in Table 1. The mean particle sizes and PDIs of the Fe_3O_4-based PLGA nanoparticles that were coated with a CS or CS-cRGD film were larger than those of the PLGA nanoparticles without a CS or CS-cRGD film. The negative zeta potential of the PLGA nanoparticles shifted to a positive zeta potential when the PLGA nanoparticles were coated with a CS or CS-cRGD film. The carrier rate of the Fe_3O_4 and the rtPA-encapsulation efficiency increased slightly after coating with a CS or CS-cRGD film.

In comparison with the control group of the Fe_3O_4−PLGA-rtPA/CS nanoparticles, the shell wavelength of the Fe_3O_4−PLGA-rtPA/CS-cRGD nanoparticles was different because of the presence of the cRGD peptide that was labeled with FITC. In a random count of 10,000 nanoparticles, there were 8,427 particles that were different from the control group; therefore, the carrier rate of the cRGD was 84.27%. The cumulative activity of the released rtPA showed that the rtPA in the Fe_3O_4−PLGA-rtPA, Fe_3O_4−PLGA-rtPA/CS, and Fe_3O_4−PLGA-rtPA/CS-cRGD nanoparticles was released slowly during the first 15 min, quickly released until 60 min, and then very slowly released with no obvious activity of the released rtPA detected from 60 to 100 min. The release of the

Table 1. Characteristics of the Fe_3O_4-Based PLGA Nanoparticles

	Fe_3O_4−PLGA	Fe_3O_4−PLGA-rtPA	Fe_3O_4−PLGA-rtPA/CS	Fe_3O_4−PLGA-rtPA/CS-cRGD
size (nm)	292.7 ± 18.7	346.2 ± 12.4	382.6 ± 10.4	395.2 ± 12.2
polydispersity index (PDI)	0.009 ± 0.003	0.097 ± 0.017	0.108 ± 0.014	0.163 ± 0.024
zeta potential (mV)	−20.3 ± 1.2	−26.2 ± 1.4	37.4 ± 1.6	29.0 ± 1.5
carrier rate of Fe_3O_4 (%)	43.7 ± 3.5	42.3 ± 2.9	51.6 ± 4.6	49.3 ± 3.4
encapsulation efficiency of rtPA (%)		54.3 ± 3.7	63.4 ± 3.3	63.7 ± 1.5

rtPA from the Fe_3O_4−PLGA-rtPA/CS and Fe_3O_4−PLGA-rtPA/CS-cRGD nanoparticles showed no significant differences at any indicated time ($P > 0.05$), whereas there were significant differences in the releases between the Fe_3O_4−PLGA-rtPA and Fe_3O_4−PLGA-rtPA/CS nanoparticles and between the Fe_3O_4−PLGA-rtPA and Fe_3O_4−PLGA-rtPA/CS-cRGD nanoparticles from 15 to 100 min ($P < 0.05$). The cumulative activity of the released rtPA from the Fe_3O_4−PLGA-rtPA nanoparticles was much lower than that from the Fe_3O_4−PLGA-rtPA/CS or Fe_3O_4−PLGA-rtPA/CS-cRGD nanoparticles (Figure 5).

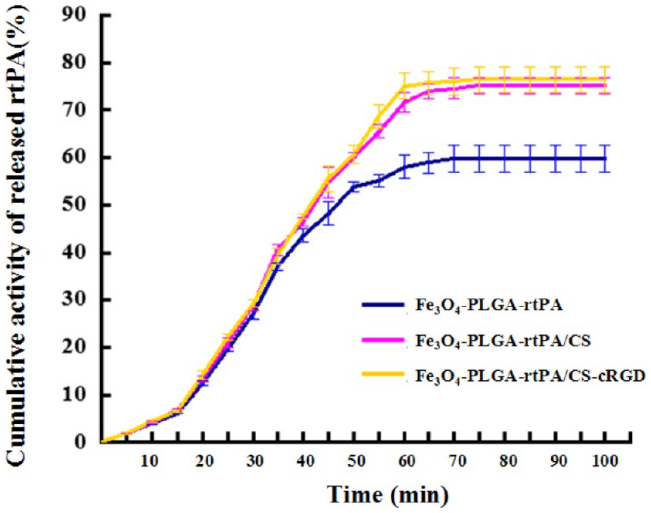

Figure 5. Profiles of the cumulative activity of the released rtPA from the Fe_3O_4−PLGA-rtPA, Fe_3O_4−PLGA-rtPA/CS, and Fe_3O_4−PLGA-rtPA/CS-cRGD nanoparticles. The cumulative release profiles indicated that the nanoparticles had a slow release phase during the first 15 min and a fast release phase until 60 min and that the highest cumulative amount of rtPA released by the Fe_3O_4−PLGA-rtPA/CS or Fe_3O_4−PLGA-rtPA/CS-cRGD nanoparticles was much higher than that released by the Fe_3O_4−PLGA-rtPA nanoparticles.

3.2. In Vitro Experiments in Targeting a Thrombus and in Thrombolysis. In the in vitro experiments in targeting a thrombus, the results of the pathological frozen section showed that a large number of the Fe_3O_4−PLGA-rtPA/CS-cRGD nanoparticles were gathered on the surface of the thrombus and that a few of the Fe_3O_4−PLGA-rtPA/CS nanoparticles were on the edge of the thrombus. There were no Fe_3O_4−PLGA or Fe_3O_4−PLGA-rtPA nanoparticles on the surface of the thrombus (Figure 6).

The changes in the weight of the thrombi in all the groups are presented in Figure 7. The differences were significant among the five groups at 15, 30, and 60 min (F = 20.514, 99.608, and 325.351, all with $P < 0.05$). The Fe_3O_4−PLGA nanoparticles induced little change in the weight of the thrombus, which demonstrated an unremarkable autolysis of the thrombus. Compared with the rates of the free rtPA solution, the thrombolysis rates of the Fe_3O_4−PLGA-rtPA, Fe_3O_4−PLGA-rtPA/CS, and Fe_3O_4−PLGA-rtPA/CS-cRGD nanoparticles improved by 1.88, 1.63, and 1.88 times at 15 min; by 2.03, 2.17, and 2.64 times at 30 min; and by 1.98, 2.41, and 3.05 times at 60 min, respectively.

3.3. MRI Characterization of the Fe_3O_4-Based PLGA Nanoparticles. The MR scan showed that the signal of each nanoparticle solution was less than that of the agarose solution, as did the SNR values, all of which confirmed that the Fe_3O_4-based PLGA nanoparticles could effectively reduce the T_2* signals (Figure 8). Although the SNR values showed significant differences among the agarose solution, the Fe_3O_4-based PLGA nanoparticles and the Fe_3O_4 solution (F = 2266.369, $P < 0.05$), there were no significant differences in the SNR values among the Fe_3O_4-based PLGA nanoparticles (F = 0.959, $P > 0.05$) and no significant differences in the SNR values between the Fe_3O_4-based PLGA nanoparticles and the Fe_3O_4 solution ($P > 0.05$) (Figure 8). The validation curves of the R_2* values of the different Fe_3O_4-based PLGA nanoparticles and the Fe_3O_4 solution are presented in Figure 9. The R_2* values increased with the concentration of Fe_3O_4 from 0.01 to 0.05 μmol/L in each Fe_3O_4-containing group. The R_2* values were not significantly different among the groups that had the same concentration of Fe_3O_4 (F = 0.339, 3.197, 2.794, 1.002, and 1.243 when the concentration of Fe_3O_4 was changed from 0.01 to 0.05 μmol/L, all with $P > 0.05$), which illustrated that the PLGA and the CS and CS-cRGD films did not affect the relaxation properties of the Fe_3O_4.

3.4. Targeting of the Thrombus and the Thrombolysis Experiments Using MRI Monitoring. The in vitro MR scan of the thrombus showed a hypointensity ring on the edge of the thrombus that was incubated with the Fe_3O_4−PLGA-rtPA/CS-cRGD nanoparticles, which indicated that the nanoparticles had gathered on the surface of the thrombus. A little hypointensity was seen on the edge of the thrombus that was incubated with the Fe_3O_4−PLGA-rtPA/CS nanoparticles, whereas no signal change was seen in the case with the Fe_3O_4−PLGA-rtPA nanoparticles (Figure 10).

The in vivo MR scan illustrated that a thrombus formed in each rat abdominal aorta. After the intravenous injection of the Fe_3O_4−PLGA-rtPA/CS-cRGD nanoparticles, the T_2 signal decreased at the mural thrombus at 10 min, the hypointensity zone widened at 20 min, and a partial vascular recanalization was detected at 40 and 60 min (Figure 11), whereas no obvious T_2 signal decrease or partial vascular recanalization was detected at the same timepoints in the rat abdominal aortas treated with the Fe_3O_4−PLGA-rtPA nanoparticles.

4. DISCUSSION

In situ thrombosis and thromboembolism are the main causes of many cardiovascular and cerebrovascular diseases.[1] The imaging of thrombi provides a wide range of possibilities to use in treatment and in improving prognoses. With the rapid development of molecular imaging, a variety of molecular probes are now available to use in targeting a throm-

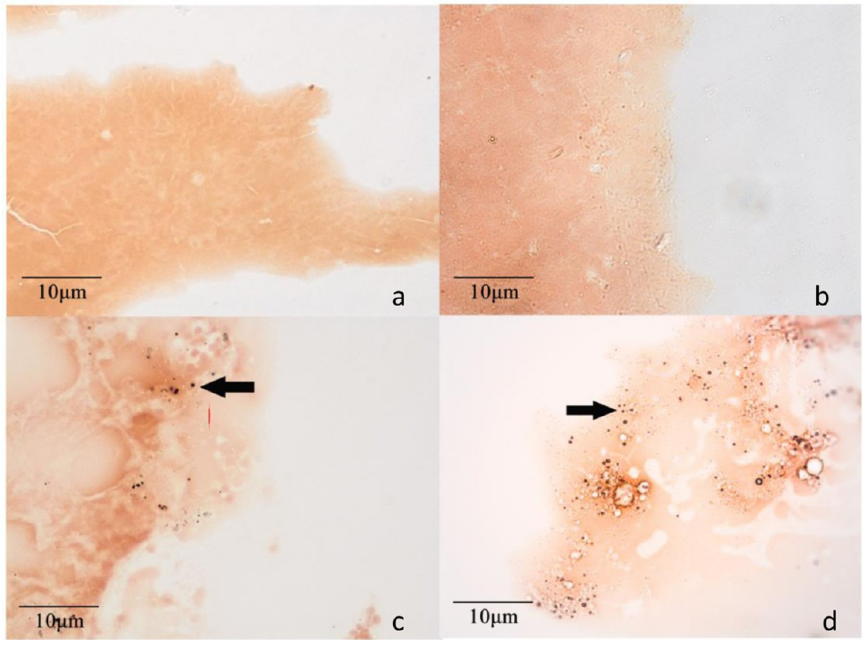

Figure 6. Pathological frozen slices of thrombi incubated with the (a) Fe_3O_4−PLGA, (b) Fe_3O_4−PLGA-rtPA, (c) Fe_3O_4−PLGA-rtPA/CS, and (d) Fe_3O_4−PLGA-rtPA/CS-cRGD nanoparticles. Many of the Fe_3O_4−PLGA-rtPA/CS-cRGD nanoparticles gathered on the surface of the thrombus, and a few nanoparticles were found in the sample with the Fe_3O_4−PLGA-rtPA/CS nanoparticles (black arrows). There were few nanoparticles gathered in the samples with the Fe_3O_4−PLGA and Fe_3O_4−PLGA-rtPA nanoparticles.

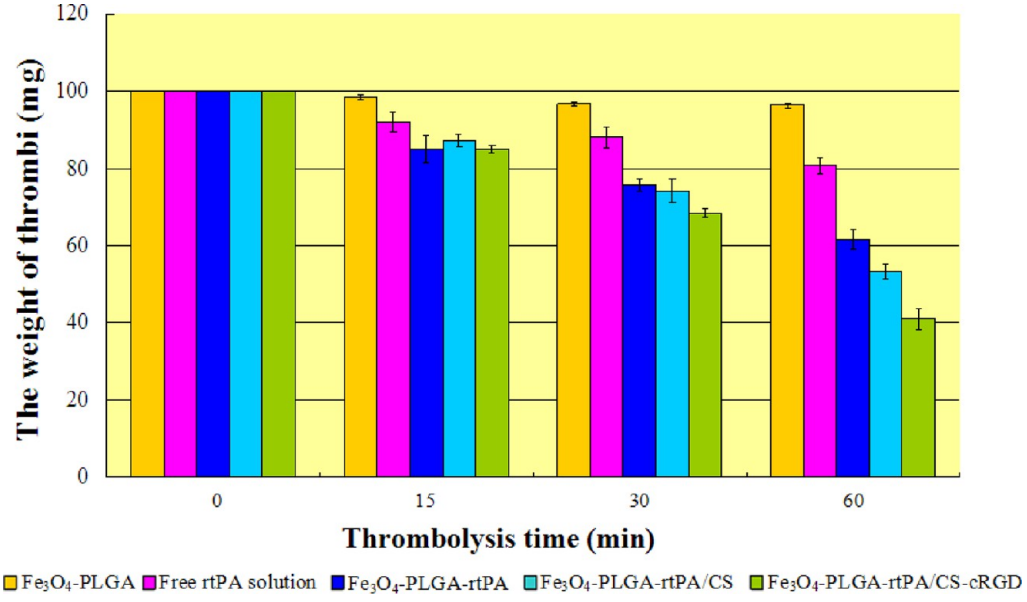

Figure 7. Weights of the thrombi at different thrombolysis times using the Fe_3O_4−PLGA nanoparticles, the free rtPA solution, and the Fe_3O_4−PLGA-rtPA, Fe_3O_4−PLGA-rtPA/CS, and Fe_3O_4−PLGA-rtPA/CS-cRGD nanoparticles. The differences were significant at 15, 30, and 60 min (F = 20.514, 99.608, 325.351, all with $P < 0.05$).

bus.[25,26,28−34] Because of its advantages of not using ionizing radiation or deep tissue penetration and of having a higher spatial resolution, MR molecular imaging has great potential in clinical applications following radionuclide imaging. Certain materials, such as MR contrast agents, targeting agents, and drugs, could be combined with special carriers using different physical and chemical methods to obtain multifunctional MR molecular probes that could be used in the early noninvasive in vivo diagnosis and treatment of various diseases at the molecular level.[35,36]

In our previous studies,[23,28] PLGA, one of the most widely used biodegradable materials, was employed as the carrier and MR contrast agent, Gd-DTPA solution, was used as the inner aqueous phase to prepare the thrombus-targeting particles. TEM confirmed that a large number of gadolinium ions filled the insides of the particles and had a uniform distribution, and the longitudinal relaxation rate could be effectively increased using a clinical MR scanner. However, because the thrombus contained iron atoms in different states at different times, the thrombus displayed a complex signal that varied with time, and it was difficult to judge precisely some parts of the thrombus in

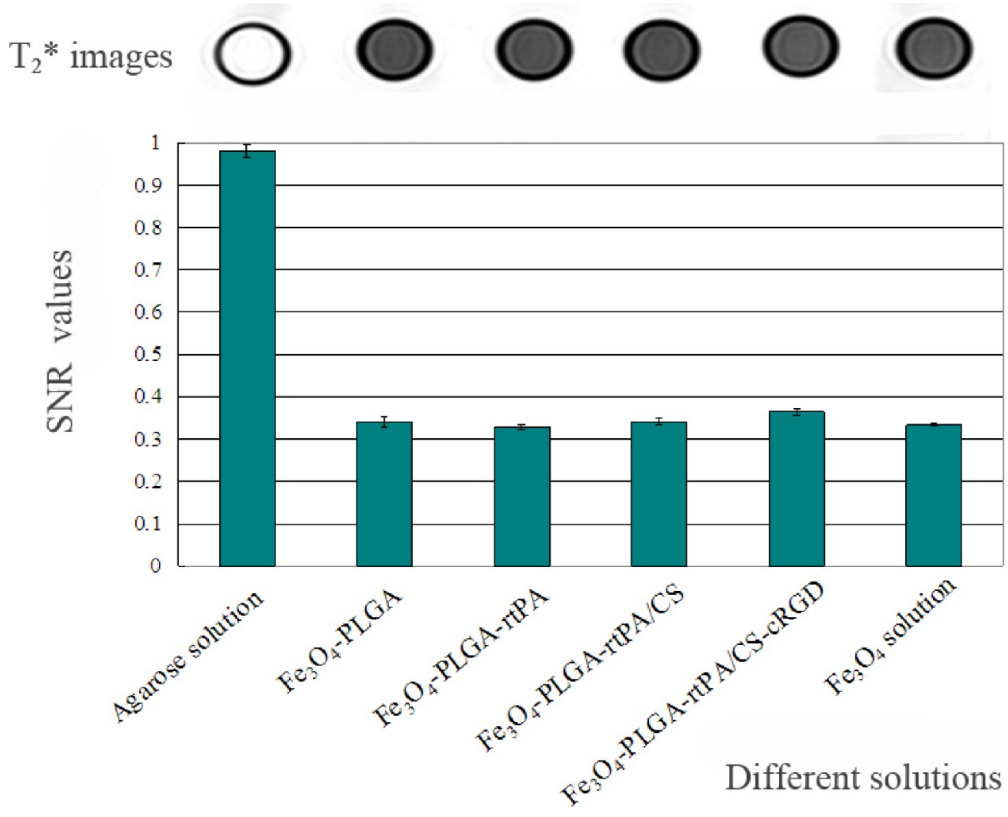

Figure 8. T_2* images and SNR values of the different solutions. Compared with the agarose solution, the Fe_3O_4-based PLGA nanoparticles effectively reduced the T_2* signals, as shown by the MR scan. There were no significant differences in the SNR values among the various Fe_3O_4-based PLGA nanoparticles and the Fe_3O_4 solution.

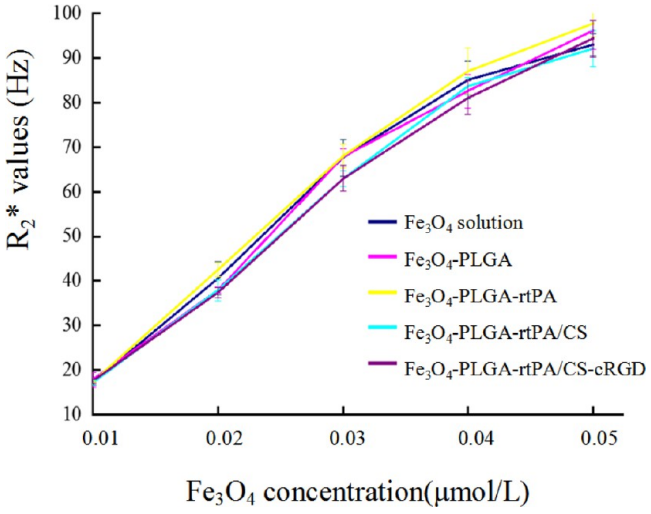

Figure 9. Validation curves of the R_2* values of the Fe_3O_4 solution, Fe_3O_4−PLGA, Fe_3O_4−PLGA-rtPA, Fe_3O_4−PLGA-rtPA/CS, and Fe_3O_4−PLGA-rtPA/CS-cRGD nanoparticles in various concentrations of Fe_3O_4 solution. The R_2* values increased with the concentration of Fe_3O_4 from 0.01 to 0.05 μmol/L, and there were no significant differences in the R_2* values among the groups at each concentration of Fe_3O_4.

vivo using only the change in the T_1 signal. Therefore, in this study, PLGA nanoparticles that were loaded with the negative MR contrast agent Fe_3O_4 were prepared to detect the thrombi, which were mainly fresh, in different periods using MRI monitoring. Simultaneously, multifunctional PLGA nanoparticles carrying the thrombolytic drug rtPA were constructed to target the thrombi and induce thrombolysis. During the process of constructing the thrombus-targeting nanoparticles, the surfaces of the iron oxide nanoparticles were modified with oleic acid, and PLGA was employed as the organic phase. TEM also showed that the Fe_3O_4 was relatively uniformly distributed in the nanospherical shell. The carrier rates of the Fe_3O_4 in the Fe_3O_4-loaded PLGA nanoparticles were 43.7, 42.3, 51.6, and 49.3%; the corresponding results suggest the likelihood of future in vitro and in vivo targeting of thrombi using the MR contrast enhancement effect. In the in vitro MR scans, the T_2* signal intensity of the Fe_3O_4-loaded PLGA nanoparticles decreased significantly compared with that of the control group. The in vitro and in vivo experiments demonstrated that the Fe_3O_4-loaded PLGA nanoparticles could be imaged on a clinical MR scanner. The R_2* value was measured instead of the R_2 value because the value of R_2 depended on the diameter of the iron oxide particle, the diffusion coefficient, and the echo space. The R_2* value of particles with a diameter of more than 10 nm (which applies to the iron oxides investigated in the present study) did not depend on these parameters. Moreover, the SIs of our MR probes at the thrombi in the pulse sequences were mainly determined by the R_2* effect of the iron oxides. Our results showed that the R_2* values increased with the concentration of Fe_3O_4 from 0.01 to 0.05 μmol/L in each Fe_3O_4-containing group and that there were no significant differences among all the groups that had the same concentration of Fe_3O_4. This result illustrated that PLGA or a CS or CS-cRGD film did not affect the relaxation properties of the Fe_3O_4. The R_2* values only depended on the concentration of the Fe_3O_4, which made the values easy to

dx.doi.org/10.1021/am406008k | ACS Appl. Mater. Interfaces 2014, 6, 5566−5576

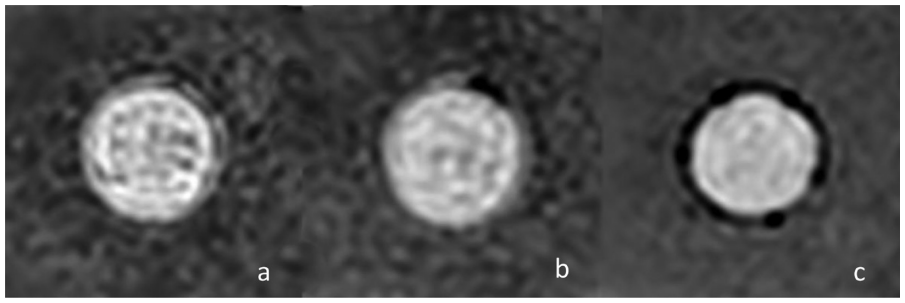

Figure 10. In vitro MR images of the targeted thrombi. The thrombi were treated with the (a) Fe_3O_4−PLGA-rtPA, (b) Fe_3O_4−PLGA-rtPA/CS, and (c) Fe_3O_4−PLGA-rtPA/CS-cRGD nanoparticles. The Fe_3O_4−PLGA-rtPA/CS-cRGD nanoparticles were deposited on the surface of the thrombus and exhibited a ring of hypointensity, and a little hypointensity could be detected on the edge of the thrombus treated with the Fe_3O_4−PLGA-rtPA/CS nanoparticles; no signal change was seen at the thrombus treated with the Fe_3O_4−PLGA-rtPA nanoparticles.

control and analyze in the MR detection of thrombi compared with the method that used Gd-DTPA, which changed the signal of tissues that had the prerequisite of contact water.

Doiron et al. confirmed that a water-soluble Gd-DTPA solution embedded in PLGA particles displayed an obvious burst release phenomenon.[17] If we first prepare the nanoparticles and then covalently bind the ligand on the surface of the nanoparticles, the burst release of the rtPA embedded in the PLGA nanoparticles will inevitably occur during the chemical reaction of the ligand and the receptor. To avoid the burst release in this study, we first prepared the CS-cRGD film using carbodiimide-mediated amide bond formation and then incorporated into the preparation procedure as one of the materials in the outer aqueous phase. Our study demonstrated that this method successfully prepared dual function PLGA nanoparticles and effectively maintained the activity of the thrombolytic drug as much as possible. At the same time, the targeting effect was clearly demonstrated in our in vitro experiments; the frozen sections of thrombus tissue demonstrated that many targeted nanoparticles aggregated around the thrombus, a result that was consistent with previous studies.[8,9,28] As an amino polysaccharide, CS has positive charges because of the protonation of its amine group. The zeta potentials of the PLGA nanoparticles changed from negative to positive after the nanoparticles were coated with a CS or CS-cRGD film, which could lead to better permeation through a negatively charged thrombus and therefore bring rtPA into the inner section of the thrombus. The frozen sections of the thrombus and the in vitro MRI targeting of the thrombus showed that nanoparticles coated with CS had a mild thrombus-targeting effect that was inferior to that of nanoparticles coated with CS-cRGD. The cRGD peptide has a good affinity with the thrombus because of its binding to a receptor antagonist of the platelet membrane glycoprotein GP IIb/IIIa, and this affinity facilitated the adhesion of the PLGA nanoparticles coated with CS-cRGD and their permeation into the thrombus. In this study, the nanoparticles coated with CS-cRGD showed higher thrombolysis rates because of the influence of the CS and cRGD than did the nanoparticles coated only with CS.

Regarding the method of carrying the thrombolytic drugs, the rtPA was connected to the surface of the nanoparticles by a chemical covalent binding method that has been reported previously and which was confirmed to be effective.[6,37] There were also literature reports showing that when rtPA was encapsulated inside the nanoparticles, the thrombolytic drugs were released via the pores on the surface of the nanoparticles or by the biodegradation of the PLGA particles and the targeting of the nanoparticles.[9,38] However, one of the major challenges to the immobilization of rtPA on the surface of the nanoparticles is the loss of its enzyme activity after immobilization.[6] It is also a time-consuming process. By contrast, the rtPA encapsulation method maintains the enzyme activity and is easy to perform. In this article, the cumulative activity of the released rtPA of the Fe_3O_4−PLGA-rtPA/CS and Fe_3O_4−PLGA-rtPA/CS-cRGD nanoparticles was much higher than that of the Fe_3O_4−PLGA-rtPA nanoparticles, which is attributed to the effect of the CS film. The nanoparticles with CS protect the enzyme activity better than do the nanoparticles without CS, which was consistent with a previous study.[8] In the in vitro thrombolysis experiment, the rtPA encapsulated into the PLGA nanoparticles showed a stronger thrombolytic efficiency compared with the free rtPA solution, which is largely attributed to the assistance with physical adhesion provided by the nanoparticles or to the active targeting ability of the nanoparticles. The sustained-release effect of the PLGA nanoparticles also plays an important role; the half-life of the rtPA was prolonged, which resulted in a lasting thrombolytic effect. This may contribute to a reduction in the use of thrombolytic drugs in clinical thrombolytic therapy and may allow a one-time-only delivery, which may reduce the complications associated with thrombolytic therapy.

Previous studies reported that an $FeCl_3$-induced arterial platelet-rich thrombus has a structure close to that of a spontaneous thrombus in a clinic.[39,40] In our study, the thrombus in the abdominal aorta formed after an injury; this was demonstrated using an MRI scan before the intravenous injection of the nanoparticles. In the in vivo thrombolysis experiment, the T_2 signal decreased at the mural thrombus at 10 min, and the hypointensity zone widened at 20 min after the intravenous injection of the Fe_3O_4−PLGA-rtPA/CS-cRGD nanoparticles; however, no obvious decrease in the T_2 signal was detected in the non-targeting group of the Fe_3O_4−PLGA-rtPA nanoparticles. This result illustrated that the Fe_3O_4−PLGA-rtPA/CS-cRGD nanoparticles targeted the surface of the thrombus. Partial vascular recanalization was detected at 40 and 60 min after the injection of the Fe_3O_4−PLGA-rtPA/CS-cRGD nanoparticles, which coincided with the results of the in vitro experiments. This result illustrated that the Fe_3O_4−PLGA-rtPA/CS-cRGD nanoparticles exhibited an effective targeted thrombolytic effect in both in vivo and in vitro experiments, as shown using MR monitoring.

There are still several limitations to this study that need to be improved in future work. First, some characteristics of the

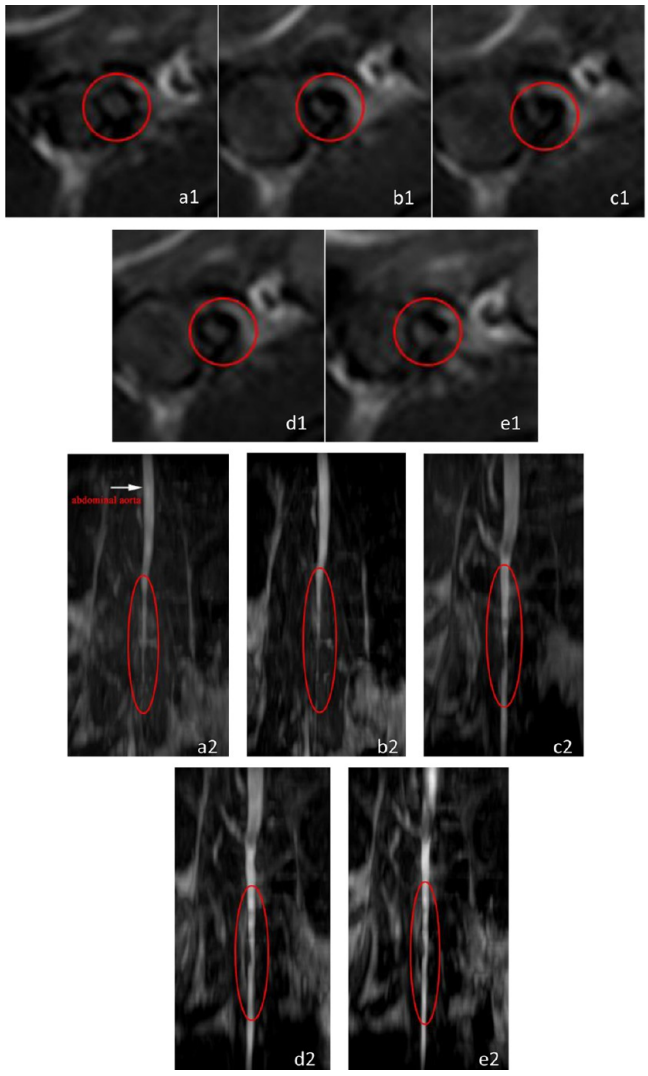

Figure 11. (a1−e1) T_2-weighted images and (a2−e2) Vs3DI images of the in vivo thrombolysis after the abdominal aorta injuries, which was monitored using MR. The images show the treatment area (a1, a2) before treatment with the intravenous Fe_3O_4−PLGA-rtPA/CS-cRGD nanoparticles and after treatment at (b1, b2) 10, (c1, c2) 20, (d1, d2) 40, and (e1, e2) 60 min. The T_2-weighted images showed a decrease in the T_2 signal at the mural thrombus and a widening of the hypointensity zone at 10 and 20 min after the intravenous injection (red circles). The Vs3DI images showed that a thrombus formed in the rat abdominal aorta and that the partial reappearance of the vessel lumen signal (red circles) was detected at 40 and 60 min.

nanoparticles need to be improved. For example, the encapsulation efficiency of the rtPA was not high enough (54.3−63.7%, which is lower than that reported in the literature (81.12%)).[2] Furthermore, the loss of enzyme activity, which leads to a non-negligible loss of activated rtPA, should be considered. The zeta potential of the nanoparticles with the CS or CS-cRGD film was too positive because of the high concentration of the samples. The nanoparticle sizes were slightly large for systemic delivery; this needs to be improved to avoid the localization of the majority of the nanoparticles in the liver and spleen. Second, we confirmed the targeting ability and thrombolytic efficiency using in vivo experiments, yet only one control group was used to demonstrate the effect of the Fe_3O_4−PLGA-rtPA/CS-cRGD nanoparticles. The pharmacokinetics of the nanoparticles and their drug distribution, metabolism, release, and biological toxicity in vivo should be studied in the future.

5. CONCLUSION

In conclusion, the Fe_3O_4-based PLGA nanoparticles constructed using the W/O/W method have a regular shape, a relatively uniform size, a high carrier rate of Fe_3O_4 and cRGD, and a high rtPA-encapsulation efficiency and activity. They have a good affinity with thrombi and exhibit strong thrombolysis and contrast-enhanced effects as seen using in vitro and in vivo experiments. They can serve as a potential dual function tool in the early detection of thrombi and in the dynamic monitoring of the thrombolytic efficiency using MRI at the molecular level.

■ ASSOCIATED CONTENT

Ⓢ Supporting Information

Optical microscope images of Fe_3O_4−PLGA, Fe_3O_4−PLGA-rtPA, Fe_3O_4−PLGA-rtPA/CS, and Fe_3O_4−PLGA-rtPA/CS-cRGD nanoparticles. This material is available free of charge via the Internet at http://pubs.acs.org.

■ AUTHOR INFORMATION

Corresponding Author

*E-mail: guodaj@163.com. Tel: +86 23 63693238,

Notes

The authors declare no competing financial interest.

■ ACKNOWLEDGMENTS

The authors are grateful to American Journal Experts (AJE) for assistance with language editing. This study was supported by the National Natural Science Foundation of China (Grant 81171332, 81130025), the Research Funds of Chongqing Bureau of Health (Grant 2011-1-052), and the Program of Chongqing University Innovation Team (Grant KJTD201303).

■ REFERENCES

(1) Whinna, H. C. Overview of Murine Thrombosis Models. *Thromb. Res.* **2008**, *122* (Suppl 1), S64−69.

(2) Hua, X.; Liu, P.; Gao, Y. H.; Tan, K. B.; Zhou, L. N.; Liu, Z.; Li, X.; Zhou, S. W.; Gao, Y. J. Construction of Thrombus-Targeted Microbubbles Carrying Tissue Plasminogen Activator and Their in Vitro Thrombolysis Efficacy: A Primary Research. *J. Thromb. Thrombolysis* **2010**, *30*, 29−35.

(3) Mu, Y.; Li, L.; Ayoufu, G. Experimental Study of the Preparation of Targeted Microbubble Contrast Agents Carrying Urokinase and RGDS. *Ultrasonics* **2009**, *49*, 676−681.

(4) Bi, F.; Zhang, J.; Su, Y.; Tang, Y. C.; Liu, J. N. Chemical Conjugation of Urokinase to Magnetic Nanoparticles for Targeted Thrombolysis. *Biomaterials* **2009**, *30*, 5125−5130.

(5) Yang, H. W.; Hua, M. Y.; Lin, K. J.; Wey, S. P.; Tsai, R. Y.; Wu, S. Y.; Lu, Y. C.; Liu, H. L.; Wu, T.; Ma, Y. H. Bioconjugation of Recombinant Tissue Plasminogen Activator to Magnetic Nanocarriers for Targeted Thrombolysis. *Int. J. Nanomed.* **2012**, *7*, 5159−5173.

(6) Chen, J. P.; Yang, P. C.; Ma, Y. H.; Wu, T. Characterization of Chitosan Magnetic Nanoparticles for in Situ Delivery of Tissue Plasminogen Activator. *Carbohydr. Polym.* **2011**, *84*, 364−372.

(7) Chen, J. P.; Yang, P. C.; Ma, Y. H.; Tu, S. J.; Lu, Y. J. Targeted Delivery of Tissue Plasminogen Activator by Binding to Silica-Coated Magnetic Nanoparticle. *Int. J. Nanomed.* **2012**, *7*, 5137−5149.

(8) Chung, T. W.; Wang, S. S.; Tsai, W. J. Accelerating Thrombolysis with Chitosan-Coated Plasminogen Activators Encapsulated in Poly-(Lactide-Co-Glycolide) (PLGA) Nanoparticles. *Biomaterials* **2008**, *29*, 228−237.

(9) Wang, S. S.; Chou, N. K.; Chung, T. W. The t-PA-Encapsulated PLGA Nanoparticles Shelled with CS or CS-GRGD Alter both

Permeation Through and Dissolving Patterns of Blood Clots Compared with t-PA Solution: An in Vitro Thrombolysis Study. *J. Biomed. Mater. Res., Part A* **2009**, *91*, 753−761.
(10) Danhier, F.; Ansorena, E.; Silva, J. M.; Coco, R.; Le Breton, A.; Préat, V. PLGA-Based Nanoparticles: An Overview of Biomedical Applications. *J. Controlled Release* **2012**, *161*, 505−522.
(11) Faisant, N.; Akiki, J.; Siepmann, F.; Benoit, J. P.; Siepmann, J. Effects of the Type of Release Medium on Drug Release from PLGA-Based Microparticles: Experiment and Theory. *Int. J. Pharm.* **2006**, *314*, 189−197.
(12) Xie, S.; Wang, S.; Zhao, B.; Han, C.; Wang, M.; Zhou, W. Effect of PLGA as a Polymeric Emulsifier on Preparation of Hydrophilic Protein-Loaded Solid Lipid Nanoparticles. *Colloids Surf., B.* **2008**, *67*, 199−204.
(13) Parveen, S.; Misra, R.; Sahoo, S. K. Nanoparticles: A Boon to Drug Delivery, Therapeutics, Diagnostics and Imaging. *Nanomedicine* **2012**, *8*, 147−166.
(14) Kocbek, P.; Obermajer, N.; Cegnar, M.; Kos, J.; Kristl, J. Targeting Cancer Cells Using PLGA Nanoparticles Surface Modified with Monoclonal Antibody. *J. Controlled Release* **2007**, *120*, 18−26.
(15) Doiron, A. L.; Homan, K. A.; Emelianov, S.; Brannon-Peppas, L. Poly (Lactic-Co-Glycolic) Acid as a Carrier for Imaging Contrast Agents. *Pharm. Res.* **2009**, *26*, 674−682.
(16) Tan, H.; Wu, J.; Lao, L.; Gao, C. Gelatin/Chitosan/Hyaluronan Scaffold Integrated with PLGA Microspheres for Cartilage Tissue Engineering. *Acta Biomater.* **2009**, *5*, 328−337.
(17) Doiron, A. L.; Chu, K.; Ali, A.; Brannon-Peppas, L. Preparation and Initial Characterization of Biodegradable Particles Containing Gadolinium-DTPA Contrast Agent for Enhanced MRI. *Proc. Natl. Acad. Sci. U. S. A.* **2008**, *105*, 17232−17237.
(18) Onuki, Y.; Jacobs, I.; Artemov, D.; Kato, Y. Noninvasive Visualization of in Vivo Release and Intratumoral Distribution of Surrogate MR Contrast Agent Using the Dual MR Contrast Technique. *Biomaterials* **2010**, *31*, 7132−7138.
(19) Lee, P. W.; Hsu, S. H.; Wang, J. J.; Tsai, J. S.; Lin, K. J.; Wey, S. P.; Chen, F. R.; Lai, C. H.; Yen, T. C.; Sung, H. W. The Characteristics, Biodistribution, Magnetic Resonance Imaging and Biodegradability of Superparamagnetic Core-Shell Nanoparticles. *Biomaterials* **2010**, *31*, 1316−1324.
(20) Yang, F.; Li, Y.; Chen, Z.; Zhang, Y.; Wu, J.; Gu, N. Superparamagnetic Iron Oxide Nanoparticle-Embedded Encapsulated Microbubbles as Dual Contrast Agents of Magnetic Resonance and Ultrasound Imaging. *Biomaterials* **2009**, *30*, 3882−3890.
(21) Akbarzadeh, A.; Mikaeili, H.; Zarghami, N.; Mohammad, R.; Barkhordari, A.; Davaran, S. Preparation and in Vitro Evaluation of Doxorubicin-Loaded Fe_3O_4 Magnetic Nanoparticles Modified with Biocompatible Copolymers. *Int. J. Nanomed.* **2012**, *7*, 511−526.
(22) Faranesh, A. Z.; Nastley, M. T.; Perez de la Cruz, C.; Haller, M. F.; Laquerriere, P.; Leong, K. W.; McVeigh, E. R. In Vitro Release of Vascular Endothelial Growth Factor from Gadolinium-Doped Biodegradable Microspheres. *Magn. Reson. Med.* **2004**, *51*, 1265−1271.
(23) Ao, M.; Wang, Z.; Ran, H.; Guo, D.; Yu, J.; Li, A.; Chen, W.; Wu, W.; Zheng, Y. J. Gd-DTPA-Loaded PLGA Microbubbles as both Ultrasound Contrast Agent and MRI Contrast Agent–A Feasibility Research. *J. Biomed. Mater. Res., Part B* **2010**, *93*, 551−556.
(24) Bellin, M. F. MR Contrast Agents, the Old and the New. *Eur. J. Radiol.* **2006**, *60*, 314−323.
(25) Huang, G.; Zhou, Z.; Srinivasan, R.; Penn, M. S.; Kottke-Marchant, K.; Marchant, R. E.; Gupta, A. S. Affinity Manipulation of Surface-Conjugated RGD Peptide to Modulate Binding of Liposomes to Activated Platelets. *Biomaterials* **2008**, *29*, 1676−1685.
(26) Srinivasan, R.; Marchant, R. E.; Gupta, A. S. In Vitro and in Vivo Platelet Targeting by Cyclic RGD-Modified Liposomes. *J. Biomed. Mater. Res., Part A* **2010**, *93*, 1004−1015.
(27) Tang, C.; Kligman, F.; Larsen, C. C.; Kottke-Marchant, K.; Marchant, R. E. Platelet and Endothelial Adhesion on Fluorosurfactant Polymers Designed for Vascular Graft Modification. *J. Biomed. Mater. Res., Part A* **2009**, *88*, 348−358.
(28) Zhang, Y.; Zhou, J.; Guo, D.; Ao, M.; Zheng, Y.; Wang, Z. Preparation and Characterization of Gadolinium- Loaded PLGA Particles Surface Modified with RGDS for the Detection of Thrombus. *Int. J. Nanomed.* **2013**, *8*, 3745−3756.
(29) Yu, X.; Song, S. K.; Chen, J.; Scott, M. J.; Fuhrhop, R. J.; Hall, C. S.; Gaffney, P. J.; Wickline, S. A.; Lanza, G. M. High-Resolution MRI Characterization of Human Thrombus Using a Novel Fibrin-Targeted Paramagnetic Nanoparticle Contrast Agent. *Magn. Reson. Med.* **2000**, *44*, 867−872.
(30) Pan, D.; Caruthers, S. D.; Hu, G.; Senpan, A.; Scott, M. J.; Gaffney, P. J.; Wickline, S. A.; Lanza, G. M. Ligand-Directed Nanobialys as Theranostic Agent for Drug Delivery and Manganese-Based Magnetic Resonance Imaging of Vascular Targets. *J. Am. Chem. Soc.* **2008**, *130*, 9186−9187.
(31) Miserus, R. J.; Herías, M. V.; Prinzen, L.; Lobbes, M. B.; Van Suylen, R. J.; Dirksen, A.; Hackeng, T. M.; Heemskerk, J. W.; van Engelshoven, J. M.; Daemen, M. J.; van Zandvoort, M. A.; Heeneman, S.; Kooi, M. E. Molecular MRI of Early Thrombus Formation Using a Bimodal Alpha2-Antiplasmin-Based Contrast Agent. *JACC Cardiovasc. Imaging* **2009**, *2*, 987−996.
(32) Unger, E. C.; Matsunaga, T. O.; McCreery, T.; Schumann, P.; Sweitzer, R.; Quigley, R. Therapeutic Applications of Microbubbles. *Eur. J. Radiol.* **2002**, *42*, 160−168.
(33) Hara, T.; Bhayana, B.; Thompson, B.; Kessinger, C. W.; Khatri, A.; McCarthy, J. R.; Weissleder, R.; Lin, C. P.; Tearney, G. J.; Jaffer, F.A. Molecular Imaging of Fibrin Deposition in Deep Vein Thrombosis Using Fibrin-Targeted Near-Infrared Fluorescence. *JACC Cardiovasc. Imaging* **2012**, *5*, 607−615.
(34) Ciesienski, K. L.; Yang, Y.; Ay, I.; Chonde, D. B.; Loving, G. S.; Rietz, T. A.; Catana, C.; Caravan, P. Fibrin-Targeted PET Probes for the Detection of Thrombi. *Mol. Pharm.* **2013**, *10*, 1100−1110.
(35) Ciesienski, K. L.; Caravan, P. Molecular MRI of Thrombosis. *Curr. Cardiovasc. Imaging Rep.* **2010**, *4*, 77−84.
(36) Gore, J. C.; Manning, H. C.; Quarles, C. C.; Waddell, K. W.; Yankeelov, T. E. Magnetic Resonance in the Era of Molecular Imaging of Cancer. *Magn. Reson. Imaging* **2011**, *29*, 587−600.
(37) Ma, Y. H.; Wu, S. Y.; Wu, T.; Chang, Y. J.; Hua, M. Y.; Chen, J. P. Magnetically Targeted Thrombolysis with Recombinant Tissue Plasminogen Activator Bound to Polyacrylic Acid-Coated Nanoparticles. *Biomaterials* **2009**, *30*, 3343−3351.
(38) Kaminski, M. D.; Xie, Y.; Mertz, C. J.; Finck, M. R.; Chen, H.; Rosengart, A. J. Encapsulation and Release of Plasminogen Activator from Biodegradable Magnetic Microcarriers. *Eur. J. Pharm. Sci.* **2008**, *35*, 96−103.
(39) Couture, L.; Richer, L. P.; Mercier, M.; Hélie, C.; Lehoux, D.; Hossain, S. M. Troubleshooting the Rabbit Ferric Chloride-Induced Arterial Model of Thrombosis to Assess in Vivo Efficacy of Antithrombotic Drugs. *J. Pharmacol. Toxicol. Methods* **2013**, *67*, 91−97.
(40) von zur Muhlen, C.; von Elverfeldt, D.; Moeller, J. A.; Choudhury, R. P.; Paul, D.; Hagemeyer, C. E.; Olschewski, M.; Becker, A.; Neudorfer, I.; Bassler, N.; Schwarz, M.; Bode, C.; Peter, K. Magnetic Resonance Imaging Contrast Agent Targeted Toward Activated Platelets Allows in Vivo Detection of Thrombosis and Monitoring of Thrombolysis. *Circulation* **2008**, *118*, 258−267.